CONSTRAINTS AS A DESTRIPING TOOL FOR HIRES IMAGES

YU CAO AND THOMAS A. PRINCE
Department of Physics, California Institute of Technology
Pasadena, CA 91125

ABSTRACT

Images produced from the Maximum Correlation Method sometimes suffer from visible striping artifacts, especially for areas of extended sources. Possible causes are different baseline levels and calibration errors in the detectors. We incorporated these factors in the MCM algorithm, and tested the effects of different constraints on the output image. The result shows significant visual improvement over the standard MCM method. In some areas the new images show intelligible structures that are otherwise corrupted by striping artifacts. And the removal of these artifacts could enhance performance of object classification algorithms. The constraints were also tested on low surface brightness areas, and were found to be effective in reducing noise level.

INTRODUCTION

The IPAC program LAUNDR invokes several one dimensional flat fielding and deglitching techniques. For the purpose of destriping the one dimensional algorithm works well for regions with a well-defined baseline, but the results is not satisfactory for regions where structure exists in all spatial frequencies (Fowler and Melnyk 1990).

Another IPAC utility KESTER, developed by Do Kester, is similar in principle to the approach we take. The idea is to process the data with YORIC to certain iterations to obtain an image, which is then used to simulate a set of detector flux measurements. The original data are then calibrated against the simulated ones.

Our approach is to combine image construction and the destriping process. Since the striping gets amplified through the iterations, the idea of applying constraints to the correction factors is natural. We investigated the possibilities of both additive and multiplicative offsets, and from our preliminary analysis it seems the multiplicative treatment is superior.

ALGORITHM

The Maximum Correlation Method can be derived based on a Maximum Likelihood scheme. Assuming a Poisson process, the likelihood function for a set of measurement D_i is

$$P = \prod_i \frac{e^{-F_i} F_i^{D_i}}{D_i!} \tag{1}$$

where F_i is the noiseless measurement value. If r_{ij} is the value of the ith footprint's response function at image pixel f_j, then

$$F_i = \sum_i r_{ij} f_j \tag{2}$$

To maximize the likelihood with estimate for f_j, we have

$$\frac{\partial \ln P}{\partial f_j} = \frac{\partial}{\partial f_j} \sum_i [-F_i + D_i \ln F_i - D_i \ln D_i + D_i] = \sum_i [-r_{ij} + r_{ij} D_i / F_i] = 0 \tag{3}$$

From this an iterative algorithm can be built (Aumann, Fowler and Melnyk 1990),

$$f_j^{(k)} = f_j^{(k-1)} C_j \tag{4}$$

where

$$\begin{aligned} C_j &= \frac{\sum_i r_{ij} C_i}{\sum_i r_{ij}} \\ &= \frac{\sum_i r_{ij} D_i / F_i}{\sum_i r_{ij}} \end{aligned} \tag{5}$$

starting from a uniform image $f_1^0 = f_2^0 = f_j^0$ for all j.

For *IRAS* data however, differing baseline and calibration exist among the detectors, which results in striping artifacts in the HiRes images. Fig. 1 (a) and (b) show the 1st and 20th iteration HiRes images for a field in the ρ Ophiuchus region at 100 μm. The input data were processed with the IPAC utility LAUNDR, [1] which applied one dimensional flat fielding to the flux measurements (Fowler and Melnyk, 1990).

We'll incorporate the estimation of leg offsets with image construction, i.e. we'll first try to maximize the likelihood function by choosing proper offsets for the legs, then proceed to compute the correction factors from the modified D_i's.

A. Assuming the offset is additive.

$D_i^* = D_i - O_L$ is the corrected measurement value. O_L is the offset, which is the same for all i's within the same scanline L.

$$P = \prod_i \frac{e^{-F_i} F_i^{D_i - O_L}}{(D_i - O_L)!} \tag{6}$$

[1] The LAUNDR'ing was carried out for a $6.5^\circ \times 6.5^\circ$ field, which was then clipped to obtain this $1^\circ \times 1^\circ$ region.

Maximizing P with choice of O_L,

$$\begin{aligned}\frac{\partial \ln P}{\partial O_L} &= \frac{\partial}{\partial O_L}\sum_{i \text{ in leg } L}[-F_i + (D_i - O_L)\ln F_i \\ &- (D_i - O_L)\ln(D_i - O_L) + (D_i - O_L)] \\ &= \sum_{i \text{ in leg } L}[-\ln F_i + \ln(D_i - O_L)] \\ &= 0 \end{aligned} \tag{7}$$

So we have,

$$\prod_{i \text{ in leg } L} \frac{D_i - O_L}{F_i} = \prod_{i \text{ in leg } L} C_i = 1 \tag{8}$$

This polynomial equation in O_L can be solved with Newton's method. O_L's are computed starting from the second iteration, since in the first iteration $F_i^0 = \sum_j r_{ij} f_j^0 = \text{const.}$ and there's no reason to regard it as an approximation of the true F_i.

B. Assuming the offset is multiplicative.

Due to calibration error in gain and the quasi-logarithmic digitization used in *IRAS*, the offset could be multiplicative in nature. In this case $D_i^* = m_L D_i$ and $\partial \ln P / \partial m_L = 0$ gives

$$\sum_{i \text{ in leg } L} D_i \ln \frac{F_i}{m_L D_i} = 0 \tag{9}$$

or

$$\prod_{i \text{ in leg } L} \left(\frac{m_L D_i}{F_i}\right)^{D_i} = \prod_{i \text{ in leg } L} C_i^{D_i} = 1 \tag{10}$$

RESULTS AND DISCUSSIONS

The test field we used is the 100 μm band of a region in ρ Ophiuchus (RA 16h23m, Dec $-23°30'$). It covers a $1.07° \times 1.07°$ field (257×257 15 arcsec pixels), with a total of 12112 footprints in 227 scanlines.

The 20th iteration image produced from method A is shown in Fig. 2(a). The calculated leg offsets are roughly Gaussian.

Corresponding image from method B is shown in Fig. 2(b). The calculated leg offsets have a deviation of 0.12.

Both Fig. 2(a) and 2(b) show significant improvement over Fig. 1(b). Striping artifacts are greatly reduced, while believable high spatial frequency features are retained. Fig. 2(a) and 2(b) have much smoother contours than Fig. 1(b).

We also notice that Fig. 2(b) is smoother than Fig. 2(a) in the high flux region. We assume the reason is that the additive offsets calculated were not able to compensate for the difference among nearby legs in the high flux region.

We carried out a simple statistical test on the nature of the leg offsets by comparing the likelihood function P obtained from the two assumptions for the

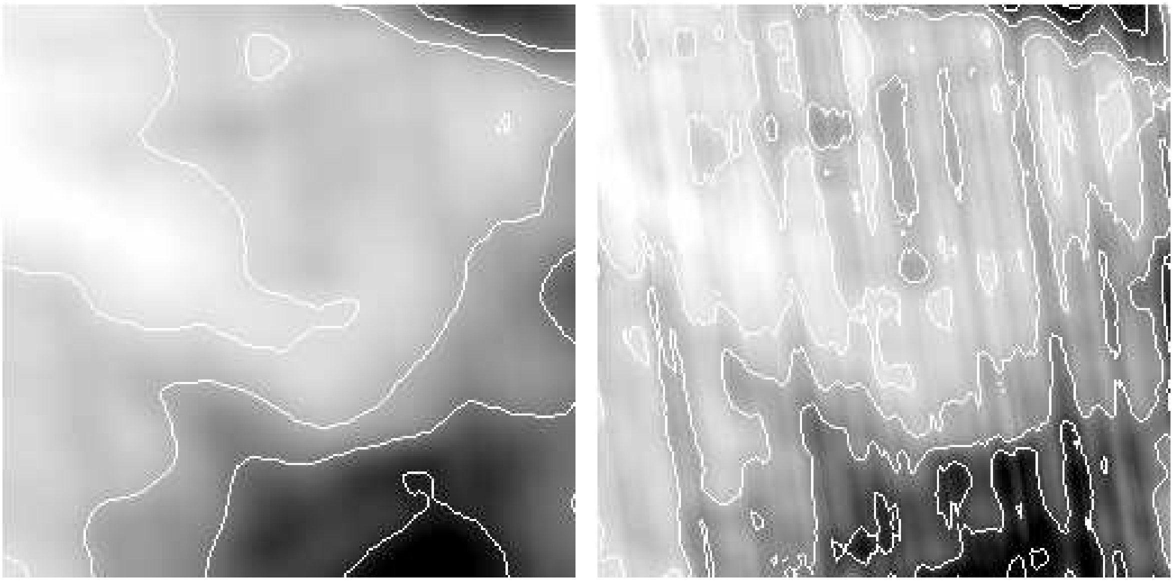

FIGURE 1 1st and 20th iteration, no offset. (Reverse video, contours start from 20th percentile, successive contours differ by factor 1.414.)

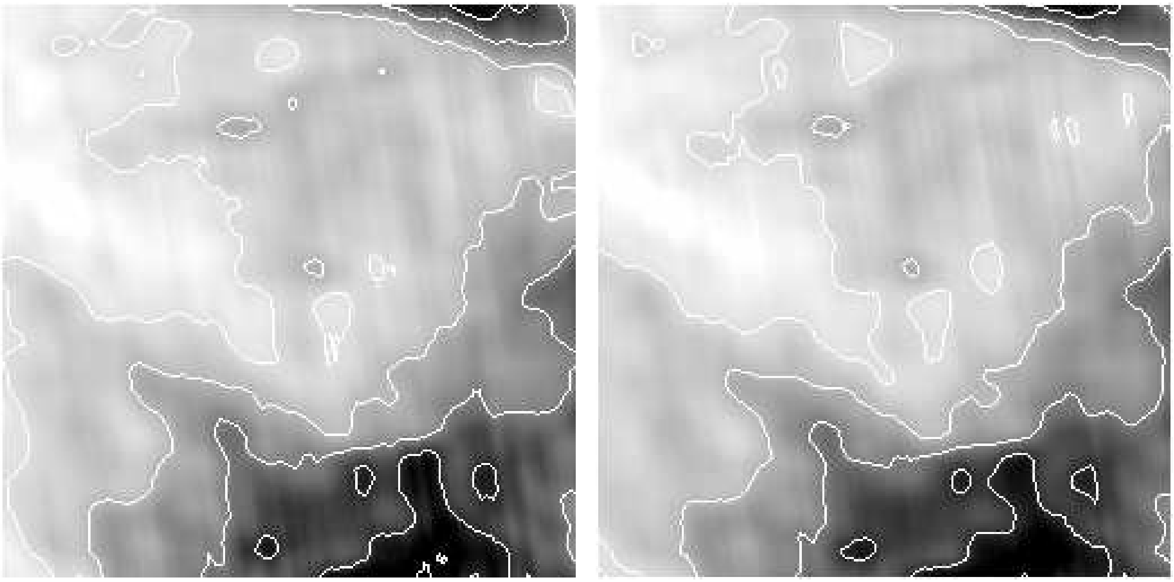

FIGURE 2 20th iteration, additive and multiplicative offsets

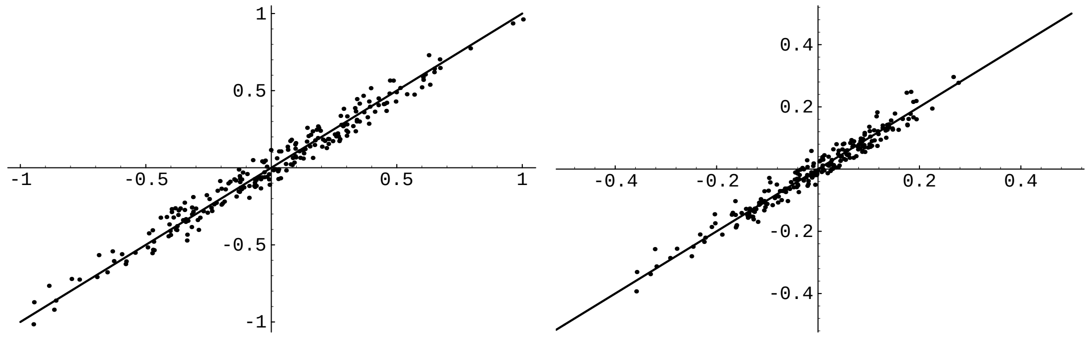

FIGURE 3 Recovery of Artificially Introduced Offsets

first calibration. The multiplicative assumption results in a bigger likelihood for 145 legs out of a total of 227. This again seems to indicate the multiplicative assumption is closer to the truth.

In addition, we tried the constrained algorithms on the 100 μm band of M101. This field features intersecting scanlines, and because of the presence of a well-defined background, is calibrated quite well with the LAUNDR program. However the constrained image shows a reduction in noise. (Figure not shown. Calculated offsets have standard deviation of 0.05).

VERIFICATION

We tested the algorithms' capability to recover offsets artificially introduced to a set of simulated detector fluxes. The detector fluxes were computed from a first iteration image of the same region, which is virtually stripe free. Gaussianly generated offsets (additive or multiplicative, magnitude being equal to that found for actual measurements) were then applied to the legs. This made-up set of detector fluxes was fed to our program, and scatter plots of the recovered vs. introduced offsets are shown in Fig. 3. (left: Y-axis: recovered additive offset, X-axis: introduced additive offset; right: Y-axis: log of recovered multiplicative offset, X-axis: log of introduced multiplicative offset.)

In the additive case, we found the residual offsets after attempt of recovery have standard deviation roughly one-sixth of that for introduced offsets, meaning a 6 fold decrease in the striping amplitude (or 15 dB decrease in power). The performance is limited by the density of the scanlines.

In the multiplicative case, the introduced offsets were Gaussian random variable with standard deviation 0.12. The standard deviation of residual offset is 0.024.

In these tests the recovered images are visually indistinguishable from the noiseless input image. This suggests that the algorithms are capable of doing what they're supposed to. So the residual striping seen in Fig. 2(a) and (b) is due to inaccuracy of the underlying assumptions about the nature of the offsets. Test runs on neighboring fields showed indeed the offsets vary considerably within each leg over the spatial scale of 1°. One of the many possible causes is the change in responsivity of the detectors when they pass through a bright source.

Our next step would be to try to understand this drifting behavior, and to incorporate it into our algorithm.

CONCLUSION

Our algorithm is just another way of trying to make use of the redundancy in the measurements. The standard HiRes processing uses it to pull out high spatial frequency information, while we take it a step further to let the scanlines calibrate each other. It resides in the same theoretical framework as the Maximum Correlation Method.

ACKNOWLEDGMENTS

We thank John Fowler and Susan Terebey for their suggestions and comments.

REFERENCES

Aumann, H. H., Fowler, J. W., and Melnyk, M. 1990, *AJ*, **99**, 1674

Fowler, J. W., and Melnyk, M. 1990, *LAUNDR Software Design Specification*, IPAC